Diamond & Related Materials 145 (2024) 111068

Contents lists available at ScienceDirect

Diamond & Related Materials

journal homepage: www.elsevier.com/locate/diamond

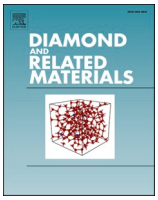

Two-dimensional diamond-diamane from graphene precursor with tilt grain boundaries: Thermodynamics and kinetics

Nuruzzaman Sakib [a], Shiddartha Paul [a,b], Keivan Davami [a], Kasra Momeni [a,*]

[a] Department of Mechanical Engineering, University of Alabama, Tuscaloosa, AL 35401, United States of America
[b] Department of Mechanical Engineering, the University of Illinois at Urbana-Champaign, Urbana, IL 61801, United States of America

A B S T R A C T

We delve into the kinetics of intricate phase transformation of graphene to atomically thin diamond, i.e., diamane, to uncover the role of grain boundary (GB) type and configuration in precursor graphene structures in determining the uniformity and transformation conditions. The occurrence of a phase transition of this nature is fundamentally associated with nanoscale dimensions, wherein the structure of graphene directly influences the thermodynamic properties. We revealed that the transformation stress, σ^t, exhibits significant dependence on both the thickness of the precursor graphene layer and the temperature. In contrast, the transformation strain, ε^t, is independent of the number of layers and type of GBs. The heterogeneous nucleation of the diamond phase within the GBs is also discovered, which differs from the interlayered nucleation and layer-by-layer transformation of diamond phases in pristine graphene.

1. Introduction

The atomically thin diamond derived from graphene has been referred to by various names in the literature. The term “diamane” [1] represents a single layer of hydrogenated graphene. Other terminologies include “diamene” [2], “diamondol” [3], “diamondene” [4], “lonsdaleite” [5], and “two-dimensional diamond” [6]. When specifically referring to a two-layered form of this diamond, terms like “bilayer diamond” [7], “bilayer graphane” [8], “diamond-like bilayer graphene” [9], and “diamondized bilayer graphene” [5] have been employed. The atomically thin diamond has exceptional properties that make it an ideal choice for high-performance electronics, specifically ones that need to operate reliably in harsh and demanding environments. It retains many hallmark characteristics of diamonds, encompassing attributes like high thermal conductivity, high mechanical strength, thermal stability, extreme hardness, and reflectivity [10,11]. Beyond these, the atomically thin diamond presents certain enhanced attributes relative to its bulk variant. These advantages include its remarkable stretchability [12–17] and low bending stiffness, 41 eV·Å^2 [18]. It also provides improved doping functionalities and a wider array of feasible dopant options, including boron [19,20], phosphorus [21], silicon [7], and sulfur [19]. These unique properties collectively underscore the immense potential of atomically thin diamonds in various technological and scientific domains, several of which have been reviewed in the literature [22,23].

Substrates play a crucial role in determining the uniformity and quality of as-grown 2D materials by affecting their kinetics [24,25]. Atomically thin diamond films have successfully been synthesized using multilayer graphene precursors by applying mechanical force (axial or shear loading), chemically assisted conversion (functionalization or substrate assisted), or combining the two [26–29]. Understanding the mechanisms governing graphene to diamane phase transformation is crucial for synthesizing high-quality diamond-based optoelectronics at industrial scales. Graphene to atomically thin diamond phase transformation mechanisms have been investigated by augmenting experimental studies with computational simulations, specifically results from ab-initio and Molecular Dynamics (MD) methods. [16,28,30–32] Several mechanisms have been proposed to describe the transformation of multilayer graphene to pristine atomically thin diamond, including direct transformation [33], transformation via nucleation [34–36], pressure-induced interlayer bonding [37], transformation via coherent interfaces [38], and shear-induced diamondization [39]. The incoherent twin boundaries are also observed in the nanodiamonds [40]. It is worth noting that the transformation mechanisms for chemically induced diamondization follow a different kinetics than the transformation to a pristine diamane [26–28,41]. A summary of atomistic mechanisms for the diamondization of graphene and graphite layers is shown in Fig. 1.

Transforming a hexagonal matrix into a cubic one and sp^2 bonds into sp^3 bonds to synthesize diamond from graphite presents significant challenges due to the high activation energy required, necessitating extreme pressures and temperatures [27,42]. However, diamond synthesis at more moderate conditions can be achieved by engineering phase transition kinetics through methods such as defect density

* Corresponding author.
E-mail address: kmomeni@ua.edu (K. Momeni).

https://doi.org/10.1016/j.diamond.2024.111068
Received 17 January 2024; Received in revised form 12 March 2024; Accepted 6 April 2024
Available online 8 April 2024

tailoring in the solid phase, compression direction, local stress state adjustments, intermediate amorphous states, and surface energy modifications [43–48]. Moreover, the role of defects in materials like graphene is crucial for phase transition and stability, where defect engineering emerges as a strategic approach to developing high-performance materials [49]. Defects provide nucleation sites essential for carbon atoms' rearrangement into a diamond's tetrahedral lattice, facilitating the breaking and forming of bonds necessary for transformation. The impact of defects, especially in facilitating chemically induced diamondization through hydrogenation, highlights the potential of defect engineering in reducing diamond synthesis costs and enhancing material performance [50–54].

Here, we investigate the kinetics of the graphene-to-diamond phase transition using the reactive MD simulation method to understand the role of GBs in the multilayer pristine graphene-to-diamond phase transitions. The developed model can be combined with other simulation methods in a multiscale framework, such as phase-field and micromechanics methods, to further investigate the role of GBs on the synthesis of atomically thin diamond films at larger length scales [55–57]. Our study demonstrates that GBs have a major impact on the kinetics of diamondization in few-layer graphene structures and the final structure and characteristics of diamane films. Furthermore, we demonstrate how the interlayer configuration of GBs affects the final structure of the formed diamane, where the formation of Moiré patterns leads to variation in the stacking of graphene layers across the sample and heterogenous transformation to diamane. Thus, GBs have the potential to form two-dimensional diamond structures composed of chemically interconnected grains with varying crystallographic orientations. It reveals new and exciting possibilities for synthesizing new 2D materials with engineered properties, which specifically can impact manufacturing novel optoelectronic devices.

2. Computational model

Graphene with Symmetric Tilt GB – Graphene is a monolayer of sp^2 hybridized carbon atoms arranged in a honeycomb lattice structure. Graphene GBs investigated in this study were created using a Voronoi-based algorithm [58–60]. Within the scope of this method, initially, a triangular lattice with appropriate orientation for the desired grain is generated. The honeycomb structure of graphene, away from the GBs, is created using a Voronoi diagram. Lloyd's algorithm [60,61] is used to construct the Centroidal Voronoi Tessellation (CVT) linked with the triangular lattice points close to the GBs. Thus, pentagon–heptagon (5|7) pairs along the GBs are obtained. After that, using the conjugate gradient method, the energy of the created structure was minimized to get the equilibrium positions of the atoms near the GBs. Constructed graphene layers with different GBs are shown in Fig. 2.

We examined multilayer graphene structures consisting of 3-, 5-, 7-, and 9 layers for each type of GB, because a minimum of 3 (ABC) stacked graphene layers is needed for the nucleation of a diamond unit cell, and any additional layer of diamond requires two additional graphene layers. Two distinct stacking arrangements were investigated: (i) *Coincident Layer Stacking* (CLS) – layer stacking that aligns the GB structures directly on top of one another in the same position, and (ii) *Offset Layer Stacking* (OLS) – layer stacking with a positional shift ensuring maximum separation between GBs in adjacent layers (Fig. 3). The dimension of the created structure in the x-axis is approximately 100 Å, and the distance between two parallel GB is 50 Å, which is more than twice the critical distance for the interaction of GBs, i.e., 20 Å [62]. The dimension in the y-axis is approximately 50 Å for all the structures created.

Interatomic Interactions – The LCBOP interatomic potential describes the interaction between carbon atoms. [63] A timestep of 0.25 fs was considered, and a Boltzmann distribution based on the set temperatures was used to initialize the atomic velocities. Statistical analysis for each case was performed using different seed numbers to initialize the velocities for the set temperatures. Subsequently, a relaxation phase was conducted under atmospheric pressure, employing the Nose-Hoover barostat [64] with a pressure-damping parameter of 1000 timesteps. Following pressure relaxation, the structures were further relaxed and maintained at a constant temperature, employing the Nose-Hoover thermostat [65] with a temperature damping parameter of 100 timesteps. Post-processing of simulation data and trajectory visualization was accomplished using OVITO and a Python script. The transformation stress, σ^t, was computed through the calculation of virial stress components.

Loading Process – The transformation of pristine graphene into

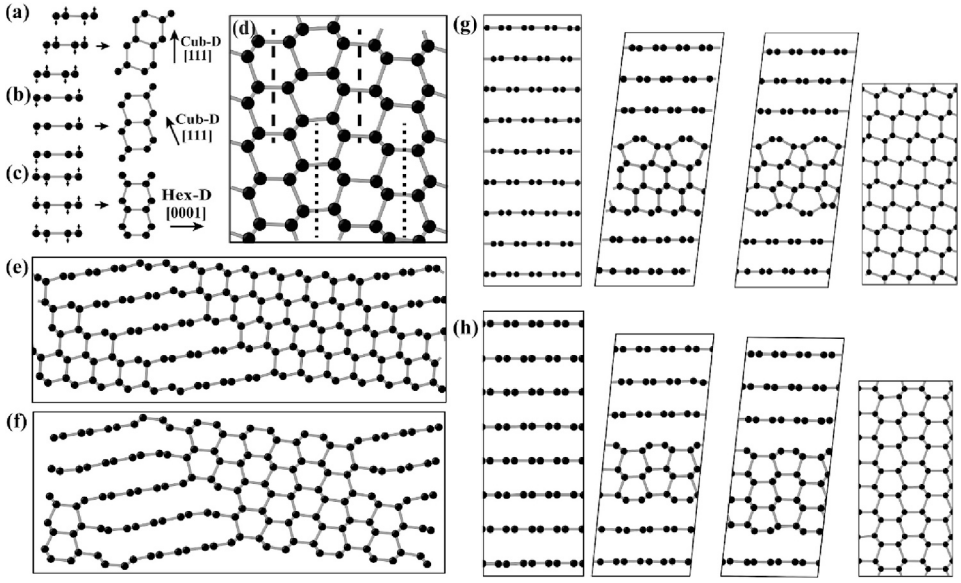

Fig. 1. Different kinetic processes for graphene to diamond transformation. (a) formation of the cubic diamond from rhombohedral graphite; transformation of orthorhombic graphite to cubic (b) and hexagonal diamond (c). [35,37](d) sp^3-coordinated diamondlike structure, which could be interpreted as either a twin-defected cubic diamond (represented by dotted lines) or a twin-defected hexagonal diamond (represented by dashed lines). [37] (e-f) diamondization via coherent graphite−diamond interfaces, i.e., Gradia. [38] Multilayer graphene to cubic (g) and hexagonal (h) diamond via nucleation in layers and growth via a layer-by-layer fashion. [36].

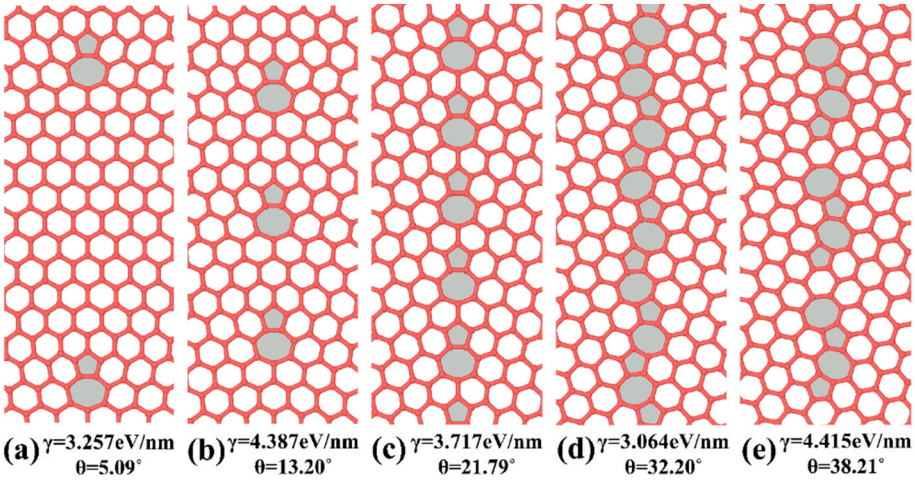

Fig. 2. Graphene structures with different GB configurations. (a) 5.09°, (b) 13.20°, (c) 21.79°, (d) 32.20°, and (e) 38.21° misoriented symmetric tilt GB of graphene.

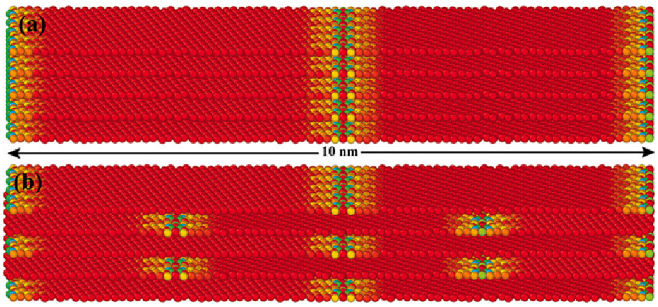

Fig. 3. Graphene layer stacking. (a) Coincident Layer Stacking (CLS) – layer stacking that aligns the GB structures directly on top of one another in the same position, and (b) Offset Layer Stacking (OLS) – layer stacking with a positional shift ensuring maximum separation between GBs in adjacent layers.

diamond typically necessitates the application of significant stress levels. In our MD simulations, the imposition of external loads was achieved by employing a hard wall model. Under this model, if an atom traverses beyond the wall's boundary during a timestep by a distance δ, it is subsequently repositioned inside the wall, offsetting the same δ distance while also reversing the sign of the corresponding velocity component. Here, two walls are positioned at a distance of 5 Å below and above the structure.

The rationale behind maintaining this specific inter-wall spacing is to provide ample room for the layered structure to undergo out-of-plane buckling relaxation during equilibration if needed. Throughout the compression phase of the simulation, the upper wall was progressively displaced toward the lower wall, maintaining a constant velocity of 1.56 $\times$ 10^{-4} Å/fs, while the lower wall retained its original position. This compression process continued until the separation between two walls fell below $c \bullet (n-1)$, where c is the bonding distance between the atoms in the diamond along the c-axis that is 2.06 Å and n is the number of layers. Subsequently, the upper wall remained stationary at this position for a duration of 25 ps before reverting to its initial configuration within an additional 37.5 ps.

3. Results and discussion

The conversion of multi-layer graphene into diamond necessitates the application of high pressure and temperature, wherein transformation stress is a pivotal parameter in signifying this diffusionless phase transition. In our simulation, we considered symmetric tilt GBs where the 5|7 defect is placed at a regular interval defined by the misorientation angle of the GBs. Within our simulation framework, we computed the transformation stress, σ^t, by evaluating the virial compressive stress along the z-direction to form 10 % diamond, consistent with the detectible diamond phase in experimental observations [27].

The transformation strain, ε^t, of the structures was calculated using the strain required to form 10 % diamond in the direction normal to graphene planes, corresponding to the loading direction, consistent with the criteria for calculating transformation stress. The reference configuration used for calculating the strain was the initial multilayer graphene setup with 3.4 Å interlayer spacing. Diamonds formed here are metastable and transformed back to multilayer graphene upon pressure release.

3.1. Diamondization of pristine graphene

Defect-free multilayer graphene structures with different numbers of layers are simulated to investigate the role of GBs on the kinetics and thermodynamics of diamane formation. In this case, with increasing compression, the layers slide and form ABC stacking, which is favorable for forming cubic diamonds. After reaching a critical pressure, the graphene layers will lock in position, and no interlayer sliding occurs upon further compression. Our results indicate that transformation stress, σ^t, of defect-free graphene to diamond increases by increasing temperature and the number of graphene layers n. We revealed that cubic diamonds form via homogenous concerted layer-by-layer transformation, similar to the previously reported graphite-to-diamond transformation captured by DFT simulations; see Fig. 1g,h. [36] These results further prove the accuracy and reliability of our simulations.

It should be noted that the current simulations assumed periodic boundary conditions within the graphene plane. In the case of graphene structures with finite size of graphene platelets, the presence of edges may result in deviation from the concerted transformation kinetics by promoting initiation of transformation from the edges. [66,67] Atoms located on the edges may go under bond relaxation and reconstruction to reduce their excess energy, or they may bond with other edge carbon atoms, creating structures like half nanotubes. Such phase transitions may promote or suppress the formation of diamane nuclei at the edges. Our MD simulations revealed that a pristine few layers (3, 5, 7, and 9) of graphene exhibit a phase transition stress normal to the c-plane of graphene within a range of 20–40 GPa (Fig. 4a or 5a). This result aligns closely with DFT simulations [68] and signifies the reliability of MD methodologies in capturing such intricate material behaviors. These results are supported by both DFT calculations [68–70] and experimental observations [71]. Specifically, previous experimental studies

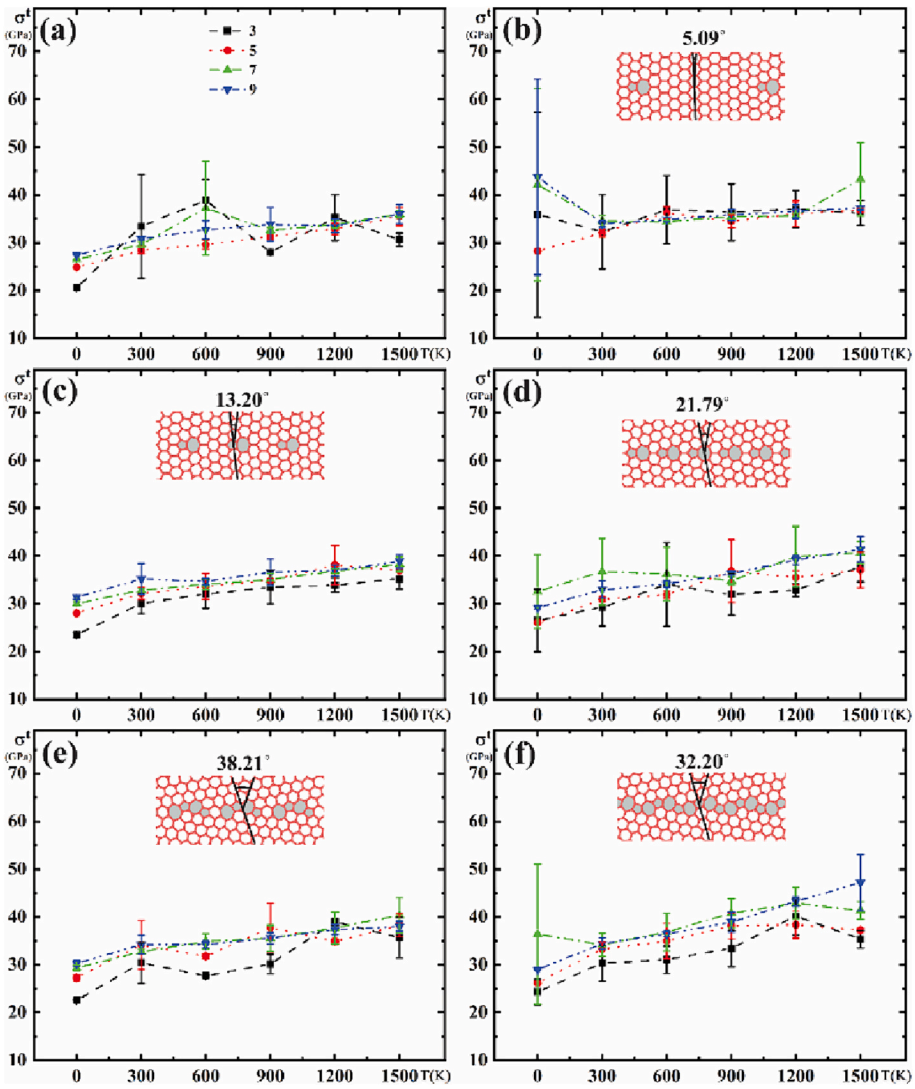

Fig. 4. Transformation stress for CLS GBs. (a) Pristine multilayer Graphene and GB structure with misorientation angle of (b) 5.09°, (c) 13.2°, (d) 21.79°, (e) 38.21°, and (f) 32.20°. σ^t increases by increasing the number of layers and shows a temperature dependence for GBs with a misorientation angle larger than 13°.

[71] have indicated transition pressures ranging from 15 GPa to 19 GPa for graphene and graphite nanoplates, respectively. Our results showcase slightly higher transition pressures, as we considered periodic boundary conditions, and the effect of edges was not present in our study. Whereas the experimental results were for the nanoplates, where the edges of the nanoplates played a key role in the nucleation of the diamond phase. This convergence between molecular dynamics simulations, DFT simulations, and experimental evidence bolsters the credibility of our findings in understanding phase transition phenomena.

3.2. GBs and transformation stress

Our exploration extends beyond pristine graphene to examine the influence of grain boundaries (GBs) on phase transitions. For GBs arranged in a CLS configuration, the transition stress along the *c*-axis spans from 20 to 40 GPa for low to mid-angle GBs and expands to 20–50 GPa for high-angle GBs. Similarly, for GBs arranged in an OLS configuration, the transition stress normal for the graphene planes ranges from 20 to 50 GPa for low to mid-angle GBs and extends from 30 to 65 GPa for high-angle GBs.

For CLS GBs, our simulation results illustrated in Fig. 4 depict the variation of transformation stress, σ^t, as a function of temperature across various misorientation angles and differing numbers of graphene layers. An increase in the number of layers corresponded to a higher σ^t value, where the error bars exhibited prominence for the 3-layered structure compared to the 5-,7- and 9-layer structures. Furthermore, the transformation stress displayed a proportional relationship with temperature, possibly attributed to thermal strains inherent in the structure. The correlation between transformation stress and the number of graphene layers is weak at room temperature and above for GB with the lowest dislocation density, Fig. 4b. Nevertheless, as the misorientation angle of the GB increases, indicating a higher dislocation density, the transformation stress exhibits a more pronounced dependence on the number of graphene layers and increases by increasing the number of layers.

For OLS GBs, a more complex correlation between transformation stress as a function of temperature and the number of layers was observed. For the perfect, pristine multilayer graphene, σ^t increases by increasing temperature and the number of graphene layers *n*. At temperatures above 300 K, Fig. 5b shows that the transformation stress remains unchanged for a low density of dislocations, regardless of the number of layers or temperature. This may be attributed to a decrease in the nucleation barrier facilitated by the stress field of dislocations.

For the GB with a tilt angle of 13.2°, Fig. 5c, σ^t increases both as a function of temp and number of graphene layers. Increasing the tilt angle to 21.79°, Fig. 5d, we revealed a decaying transformation stress vs. temperature relationship. Also, while at σ^t is inversely proportional to

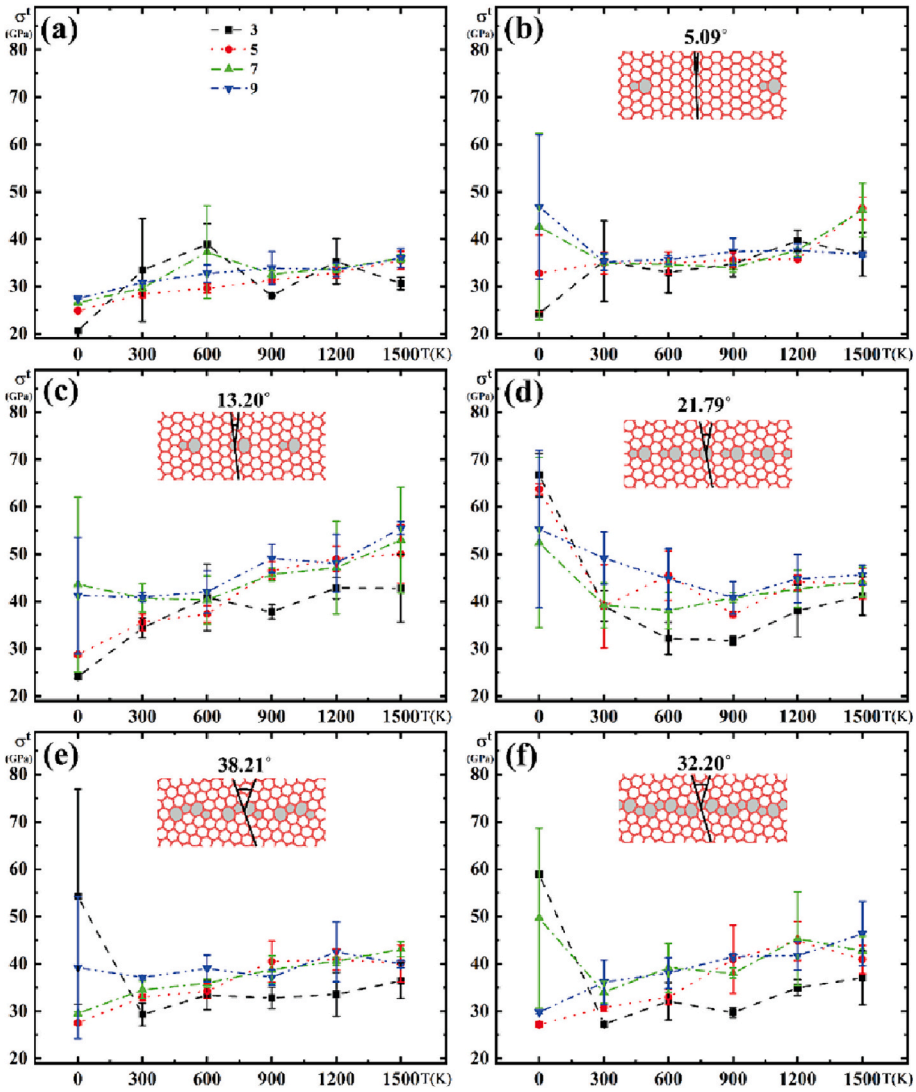

Fig. 5. Transformation stress for OLS GBs. (a) Pristine multilayer Graphene and GB structure with misorientation angle of (b) 5.09°, (c) 13.2°, (d) 21.79°, (e) 38.21°, and (f) 32.20°. σ^t increases by increasing the number of layers, except for GBs with moderate tilt angle of 21.79° at low temperatures. A weak temperature dependence is also revealed for diamondization of pristine multilayer graphene structures without GBs, as well as ones with low and high tilt angles.

the number of graphene layers at 0 K; this trend reverses for temperatures above 300 K, where σ^t will be minimum for 3 L graphene structures, while for higher temperatures, the difference in transformation stresses for 5 L+ graphene structures become negligible. In the case of 38.21° tilt angle, Fig. 5e, transformation stress is proportional to temperature and increases with the number of layers up to 900 K, beyond which it becomes independent of n for 5 L+ graphene structures. Finally, for 32.20° tilt angle with the highest dislocation density, Fig. 5f, σ^t shows an increasing relationship with temperature. While σ^t is minimum for the 3 L system, it will be independent of n for 5 L+ structures.

3.3. GBs and transformation strain

Transformation strains for CLS GBs and OLS GBs are shown in Figs. 6 and 7, respectively. Our analyses reveal that ε^t remains unaffected by variations in T and the count of graphene layers, n, in pristine configurations. For CLS multilayer graphene configurations, the 3 L graphene structure has a slightly higher transformation strain than the rest of the structures for multilayer GBs with low-angle GBs (Fig. 6b, c). The highest uncertainty in calculating ε^t is associated with the 3 L configuration. Acknowledging this uncertainty leads to the inference that ε^t is independent of T and n across all CLS configurations. This observation lends credence to previously documented claims regarding the temperature-insensitivity of transformation strain, [27,72] reinforcing the credibility of ε^t as a robust metric for discerning structural transformations.

The transformation strain for OLS GBs, Fig. 7, is independent of temperature for multilayer graphene structures devoid of GBs and structures with low and high tilt angles. However, for structures with an intermediate tilt angle, Fig. 7d, ε^t exhibits a nonlinear dependency on temperature T. Specifically, ε^t decreases with increasing T up to 600 K, beyond which it plateaus. Additionally, it is noteworthy that the transformation strain, ε^t, remains largely unaffected by the count of graphene layers, n. Consequently, the GB misorientation angle becomes a pivotal determinant for phase transformation conditions, especially in GBs with intermediate tilt angles and at mid-range temperatures.

Upon examining the transformation strain, ε^t, for both CLS and OLS configurations with varying graphene layer counts at different temperatures, it is evident that for the CLS configurations, ε^t increases upon introducing GBs. Interestingly, ε^t does not show dependency on either n and T for pristine and CLS configurations with low misorientation angles, and for moderate and high misorientation GBs it is only a weak linear function of temperature. In the context of OLS configurations, ε^t is independent or only a weak function of temperature for pristine

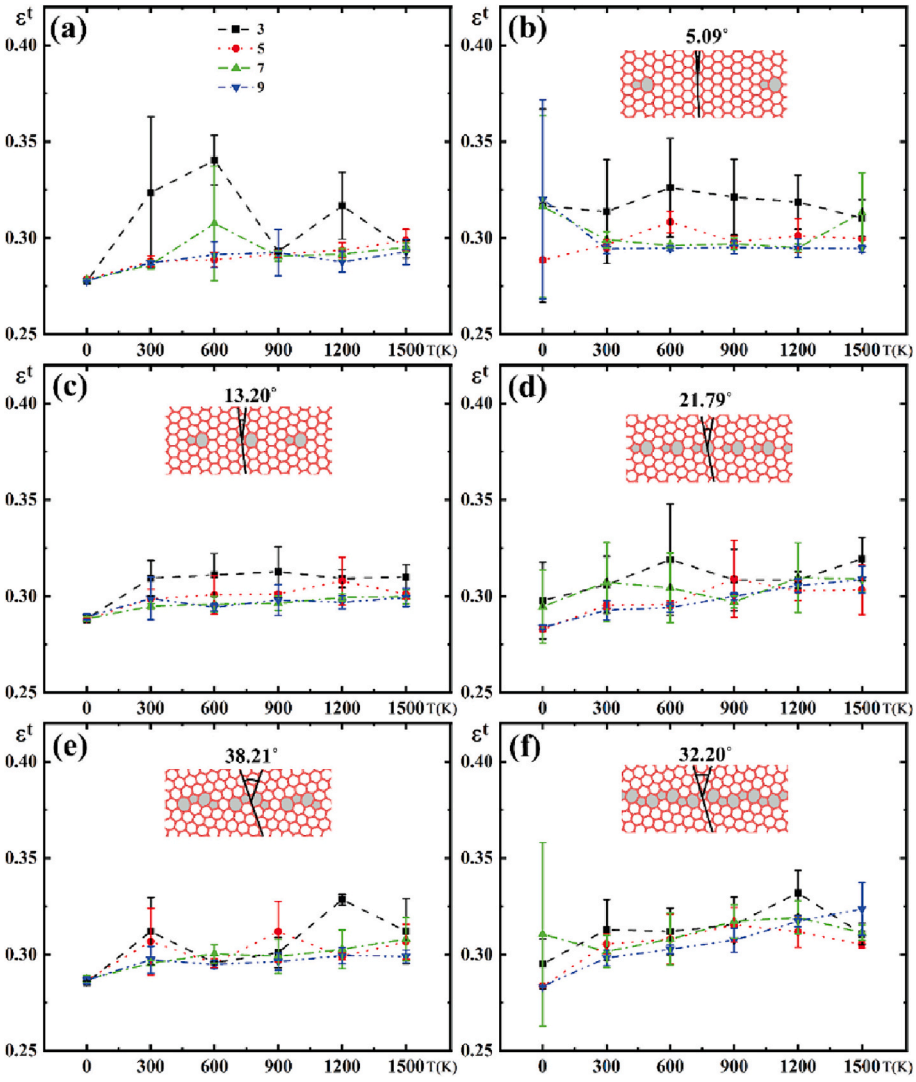

Fig. 6. Transformation strain for CLS GBs. (a) Pristine multilayer Graphene and GB structure with misorientation angle of (b) 5.09°, (c) 13.2°, (d) 21.79°, (e) 38.21°, and (f) 32.20°. The results indicate the independence of transformation strain from temperature *T* and the number of graphene layers *n*.

graphene and ones with low and high tilt angles. However, it shows a nonlinear decaying response for moderate tilt angles, which plateaus beyond 600 K.

3.4. Transformation kinetics

Elucidating the nucleation mechanisms at the nanoscale is pivotal for enhancing the phase transition from graphene to diamane on a large scale. A myriad of transformation mechanisms for pristine graphite have been postulated, as delineated in Fig. 1. Nonetheless, the influence of defects on the kinetics of the graphene-to-diamane transformation remains uncharted territory. Existing literature predominantly focuses on the impact of point defects during the chemically induced phase transition from graphene to diamane. Notably, studies have indicated that vacancies and 5|7 defects serve as preferential sites for hydrogenation, [54] with vacancies exerting a more pronounced influence on the diamondization process. Such defects are instrumental as nucleation sites during the chemically induced diamondization. Here, we revealed the pivotal role of GBs on the kinetics of diamondization of few-layer graphene structures.

The kinetics of diamondization for the 3 L graphene structure with low-angle tilt GB (Fig. 2a) with 5|7 defect is shown in Fig. 8. Initially, the layers were stacked in AA stacking with GBs placed in the same position for CLS configuration, Fig. 3a. Then the layered structure was compressed, and as a result, the out-of-plane buckling due to GBs (Fig. S5a in Supplemental Materials) in the graphene layer flattened out. At this point, the CLS GBs get the ABA stacking by sliding the layer under compressive stress (Fig. S5b in Supplemental Materials). With further compression, the stacking changed to ABCA stacking (Fig. S5c in Supplemental Materials), and cubic diamond nucleates in the GB area at 21.5 GPa, Fig. 8a, driven by the relaxation of the GB energy. After that, with increasing compressive stress, homogeneous (random and spontaneous) nucleation starts without any preferential sites. Still, it is separated by a distance commensurate with the spacing between dislocations, Fig. 8b. The formed diamond nuclei will grow along the armchair direction (red arrow in Fig. 8c. Further growth in another armchair direction at a 60°-inclined angle, marked by red arrows in Fig. 8d, initiates as the diamondized regions get close to the GB region, indicating the potential role of elastic energy on diamondization kinetics of few-layer multi-grain graphene structures.

The diamondized regions grow and coalesce, as marked by red ovals in Fig. 8e. The merged regions will continue to grow till the complete transformation of multilayered graphene to diamond at 30 GPa. However, the core of dislocations in the GB region, i.e., 5|7 defects, did not transform into a diamond even after the complete transfer of graphene multilayers, Fig. 8f, forming only partial sp^2 to sp^3 structural alterations.

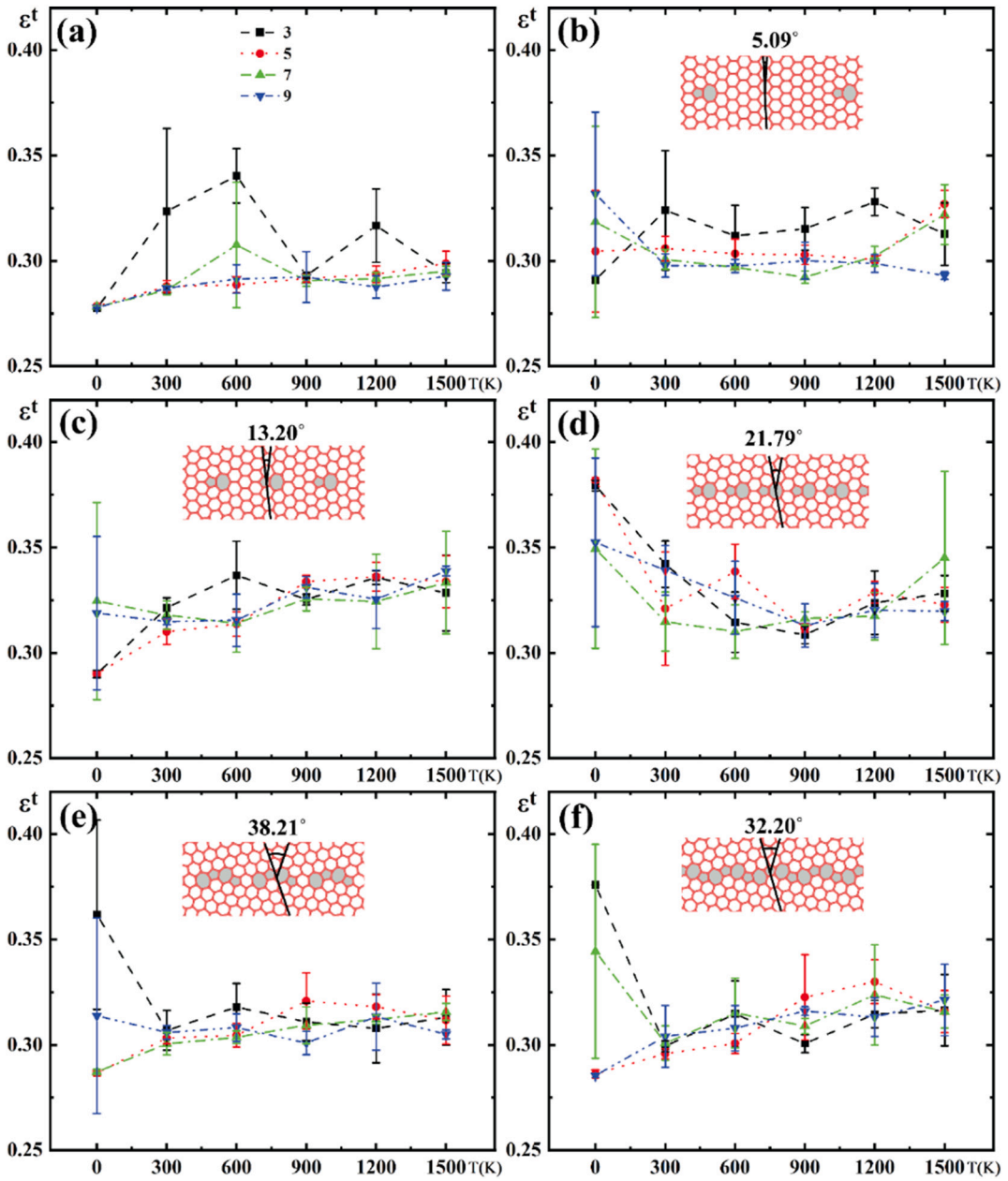

Fig. 7. Transformation strain for OLS GBs. (a) Pristine multilayer Graphene, and GB structure with misorientation angle of (b) 5.09°, (c) 13.2°, (d) 21.79°, (e) 38.21°, and (f) 32.20°. Transformation strain is independent of T and n.

For OLS GBs where GBs are placed in an alternating position in the adjacent layers, Fig. 2b, the relaxed structure wrinkled around the 5|7 defects in the GB region (Fig. S6a in Supplementary Information). The structure forms Moiré patterns that are more visible upon compression when the wrinkles flatten. The formation of a Moiré pattern occurs when two copies of a periodic pattern are superimposed on one another with a relative rotation. The heterogeneous nucleation starts from the GB region in the middle layer, Fig. 9a, which then grows within the GB till another nucleation starts within the GB in the top and bottom layers, Fig. 9b. The formed diamane nuclei grow out of the GB region, Fig. 9c, and they coalesce and form larger transformed areas across multiple layers, Fig. 9d. The merging diamane regions are marked with red oval in Fig. 9e. The structure then continues to transform into diamane till it reaches GBs, where it forms a hexagonal diamond close to 5|7 defects in GBs, Fig. 9f.

Comparison of the final diamane structures formed from the CLS and OLS configurations, Figs. 8f and 9f, indicate the major role of GB configuration across different layers on the final structure and transformation stress of the formed diamane. While the multilayer defected graphene in CLS configuration transformed completely to diamond at ~30 GPa, except for small regions close to 5|7 defects, the non-transformed region in the OLS configuration is almost as large as the entire GB even at ~40 GPa. The initial OLS multilayer graphene, after the GBs are flattened due to the compressive pressure, shows three different stacking AA, AB, and AC in the structure. Cubic diamond nucleates from AB stacked layers by forming ABC stacking at high pressure with relative sliding of the layers. The AA stacked region can help to nucleate the hexagonal diamond (lonsdaleite). Furthermore, while we could only observe cubic diamond structure in the diamane structure formed from the initial CLS graphene configuration, hexagonal diamond formed close to the 5|7 defects in the case of the OLS graphene structures. Videos of diamondization kinetics for pristine, CLS, and OLS structures are included in supplementary materials.

Initiation of diamondization from the GB region can be described

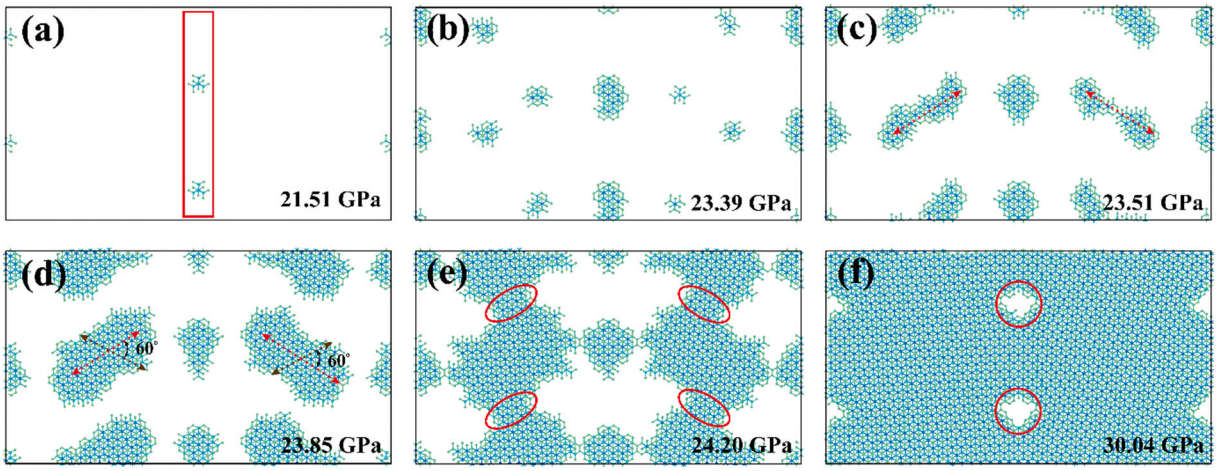

Fig. 8. Phase transformation mechanisms in CLS GB position for 5.09° misoriented GB at 0.5 K. Diamondization starts via heterogeneous nucleation in the GB region marked by the red rectangle (a), followed by random spontaneous homogenous nucleation with the region between GBs (b). Diamond nuclei grow along the armchair direction (marked as red) (c) till they get close to GB, where they switch their growth direction to 60° to another armchair (marked by a blue line) (d). Different diamondized regions will then merge (red oval regions) (e) and grow to form a single crystalline diamane (f) with trapped non-transformed regions in the dislocation dipole area (marked in red).

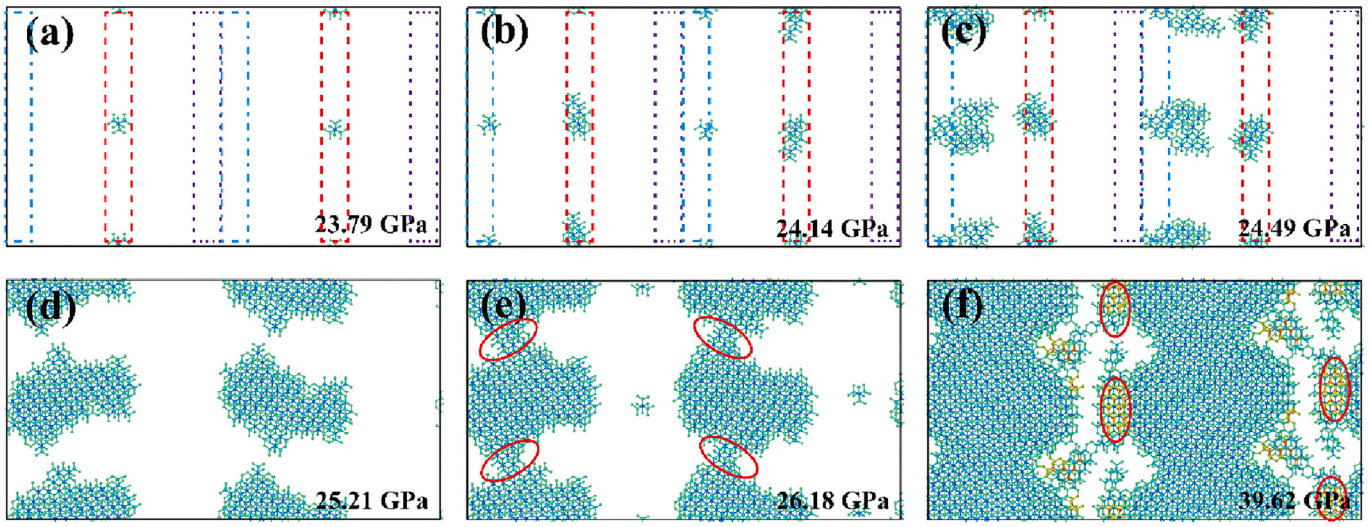

Fig. 9. Phase transformation mechanisms in OLS GB position for 5.09° misoriented GB at 0.5 K. Diamondization starts via heterogeneous nucleation in (a) the GB region of middle layer marked by the red dashed rectangle, followed by nucleation in (b) GB regions of the top (blue dash-dot line) and bottom (Purple dotted line) layers. Nucleated diamond regions grow outside of the GB region (c,d) till they coalesce (e), marked by red oval regions. Finally, the multilayer graphene structure transforms to diamond completely, except close to the 5|7 defects in the GB. Hexagonal diamond forms close to the 5|7 defects, which are marked by red solid oval regions in (f).

based on the excess GB energy and the interfacial stresses present at the GBs due to the mismatch strain between the adjacent grains. Considering the energy barrier for the transformation of graphene to diamane to be $\Delta E + P \bullet \Delta V$, where ΔE is the transformation energy barrier, P is pressure, and ΔV is the activation volume and is negative for different diamondization pathways [36]. Thus, upon increasing pressure (stresses), the contribution of $P \bullet \Delta V$ term increases (with a maximum at GBs due to additional mismatch stresses) till it exceeds ΔE, above which diamondization happens spontaneously.

4. Conclusions

In our study, we explored the transformation of multilayered graphene into diamane using a computational model based on the reactive MD technique, focusing on the effects of symmetric tilt GBs, temperature, and the number of graphene layers. Our findings indicate a proportional relationship between transformation stress and temperature in pristine multilayer graphene, which escalates with an increase in graphene layers, highlighting the influence of thermal strains. The investigation into configurations with CLS and OLS GBs revealed that transformation stress values increase with layer count and are proportional to temperature, with notable effects from dislocation densities on the stress response. Additionally, our research shows that at temperatures above 300 K, OLS configurations maintain consistent transformation stress levels for low dislocation densities, suggesting reduced nucleation barriers due to dislocation stress fields, while moderate tilt angles in GBs show a declining stress-temperature relationship that stabilizes beyond 600 K.

Regarding transformation strain, we observed negligible variation in CLS multilayer graphene configurations across different temperatures and layer counts, whereas OLS grain boundaries maintained a steady transformation strain irrespective of these factors, except at moderate

misorientation angles, which showed a nonlinear decrease in strain, stabilizing beyond 600 K. The transformation mechanisms differ between pristine graphene and multilayer graphene bi-grain structures; pristine graphene undergoes a homogeneous layer-by-layer transformation to cubic diamane, whereas bi-grain structures transform through heterogeneous nucleation at GBs, leading to the formation of diamond nuclei and subsequent coalescence into diamane. However, diamond formation faces obstructions in areas with 5|7 defects in CLS configurations and along GBs in OLS configurations due to Moiré patterns and defect presence. It leads to a heterogeneous structure of cubic, hexagonal, and non-transformed graphene, with ABC stacking in CLS configurations favoring cubic diamond formation and diverse stackings in OLS, leading to varied energy landscapes and phase transformations.

In summary, the results presented here can guide the synthesis of diamane structures. The preferred choice for economically synthesizing diamane using stress-controlled processes is the CLS configuration due to its generally lower transformation stress than the OLS configuration. In contrast, transformation strain remains relatively independent of the number of layers, making strain-controlled processes the preferred option. Additionally, the CLS configuration with GBs results in a higher volume fraction of diamane at lower pressures, making it the favorable choice for producing high-quality diamonds. However, it's worth noting that only the OLS configuration leads to the formation of hexagonal diamonds, so if a hexagonal diamond is required for a specific application, selecting the OLS configuration is necessary.

Supplementary data to this article can be found online at https://doi.org/10.1016/j.diamond.2024.111068.

CRediT authorship contribution statement

Nuruzzaman Sakib: Writing – original draft, Visualization, Validation, Software, Methodology, Investigation, Formal analysis, Conceptualization. **Shiddartha Paul:** Writing – review & editing. **Keivan Davami:** Writing – review & editing. **Kasra Momeni:** Writing – review & editing, Writing – original draft, Supervision, Resources, Funding acquisition, Conceptualization.

Declaration of competing interest

The authors declare that they have no known competing financial interests or personal relationships that could have appeared to influence the work reported in this paper.

Data availability

Data will be made available on request.

Acknowledgment

This project is supported by the NSF-CAREER under the NSF cooperative agreement CBET-2042683.

References

[1] L.A. Chernozatonskii, P.B. Sorokin, A.G. Kvashnin, D.G. Kvashnin, Diamond-like C_2H nanolayer, diamane: simulation of the structure and properties, JETP Lett. 90 (2009) 134–138, https://doi.org/10.1134/S0021364009140112.

[2] F. Cellini, F. Lavini, T. Cao, W. de Heer, C. Berger, A. Bongiorno, E. Riedo, Epitaxial two-layer graphene under pressure: Diamene stiffer than diamond, FlatChem 10 (2018) 8–13, https://doi.org/10.1016/j.flatc.2018.08.001.

[3] A.P.M.M. Barboza, M.H.D.D. Guimaraes, D.V.P.P. Massote, L.C. Campos, N. M. Barbosa Neto, L.G. Cancado, R.G. Lacerda, H. Chacham, M.S.C.C. Mazzoni, B.R. A.A. Neves, Room-temperature compression-induced diamondization of few-layer graphene, Adv. Mater. 23 (2011) 3014–3017, https://doi.org/10.1002/adma.201101061.

[4] L.G.P. Martins, M.J.S.S. Matos, A.R. Paschoal, P.T.C.C. Freire, N.F. Andrade, A. L. Aguiar, J. Kong, B.R.A.A. Neves, A.B. De Oliveira, M.S.C.C. Mazzoni, A.G.S. S. Filho, L.G. Cançado, L.G. Cançado, L. Gustavo, P. Martins, M.J.S.S. Matos, A. R. Paschoal, P.T.C.C. Freire, N.F. Andrade, A.L. Aguiar, J. Kong, B.R.A.A. Neves, A. B. De Oliveira, M.S.C.C. Mazzoni, A.G.S.S. Filho, L.G. Cançado, Raman evidence for pressure-induced formation of diamondene, Nat. Commun. 8 (2017) 96, https://doi.org/10.1038/s41467-017-00149-8.

[5] T. Pakornchote, A. Ektarawong, B. Alling, U. Pinsook, S. Tancharakorn, W. Busayaporn, T. Bovornratanaraks, Phase stabilities and vibrational analysis of hydrogenated diamondized bilayer graphenes: a first principles investigation, Carbon N. Y. 146 (2019) 468–475, https://doi.org/10.1016/j.carbon.2019.01.088.

[6] L.S. Li, X. Zhao, Transformation between different hybridized bonding structures in two-dimensional diamond-based materials, J. Phys. Chem. C 115 (2011) 22168–22179, https://doi.org/10.1021/jp205271x.

[7] D. Qiu, Q. Wang, S. Cheng, N. Gao, H. Li, Electronic structures of two-dimensional hydrogenated bilayer diamond films with Si dopant and Si-V center, Results Phys. 13 (2019) 102240, https://doi.org/10.1016/j.rinp.2019.102240.

[8] O. Leenaerts, B. Partoens, F.M. Peeters, Hydrogenation of bilayer graphene and the formation of bilayer graphane from first principles, Phys. Rev. B 80 (2009) 245422, https://doi.org/10.1103/PhysRevB.80.245422.

[9] Y. Hu, D. Li, Y. Yin, S. Li, G. Ding, H. Zhou, G. Zhang, The important role of strain on phonon hydrodynamics in diamond-like bi-layer graphene, Nanotechnology 31 (2020) 335711, https://doi.org/10.1088/1361-6528/ab8ee1.

[10] A.M. Bonnot, B.S. Mathis, S. Moulin, Investigation of the growth kinetics of low pressure diamond films by in situ elastic scattering of light and reflectivity, Appl. Phys. Lett. 63 (1993) 1754–1756, https://doi.org/10.1063/1.110704.

[11] B. Liu, E. Emmanuel, T. Liang, B. Wang, Advancements in theoretical and experimental investigations on diamane materials, Nanoscale 15 (2023) 10498–10512, https://doi.org/10.1039/D3NR01400B.

[12] B. Mortazavi, F. Shojaei, B. Javvaji, M. Azizi, H. Zhan, T. Rabczuk, X. Zhuang, First-principles investigation of mechanical, electronic and optical properties of H-, F- and Cl-diamane, Appl. Surf. Sci. 528 (2020) 147035, https://doi.org/10.1016/j.apsusc.2020.147035.

[13] A.S. Machado, D. Maroudas, A.R. Muniz, Tunable mechanical properties of diamond superlattices generated by interlayer bonding in twisted bilayer graphene, Appl. Phys. Lett. 103 (2013) 013113, https://doi.org/10.1063/1.4813271.

[14] P.R. Niraula, T. Cao, A. Bongiorno, Mechanical properties of sp^3-bonded carbon and boron nitride 2D membranes: a first principles study, Comput. Mater. Sci. 179 (2020) 109635, https://doi.org/10.1016/j.commatsci.2020.109635.

[15] Y.-C. Wu, J.-L. Shao, Z. Zheng, H. Zhan, Mechanical properties of a single-layer Diamane under tension and bending, J. Phys. Chem. C 125 (2021) 915–922, https://doi.org/10.1021/acs.jpcc.0c08172.

[16] A.R.R. Muniz, A.S.S. Machado, D. Maroudas, Mechanical behavior of interlayer-bonded nanostructures obtained from bilayer graphene, Carbon N. Y. 81 (2015) 663–677, https://doi.org/10.1016/j.carbon.2014.10.003.

[17] S.K. Tiwari, R. Pandey, N. Wang, V. Kumar, O.J. Sunday, M. Bystrzejewski, Y. Zhu, Y.K. Mishra, Progress in diamanes and diamanoids nanosystems for emerging technologies, Adv. Sci. 9 (2022) 2105770, https://doi.org/10.1002/advs.202105770.

[18] S. Jiang, L. Sun, H. Zhan, Z. Zheng, X. Peng, C. Lü, Bending behavior of diamane and twisted bilayer graphene: insights from four-point bending deformation, Thin-Walled Struct. 195 (2024) 111415, https://doi.org/10.1016/j.tws.2023.111415.

[19] M. Fyta, Nitrogen-vacancy centers and dopants in ultrathin diamond films: electronic structure, J. Phys. Chem. C 117 (2013) 21376–21381, https://doi.org/10.1021/jp407356u.

[20] C. Niu, Y. Cheng, K. Yang, J. Zhang, H. Zhang, Z. Zeng, X. Wang, Boron-dopant enhanced stability of diamane with tunable band gap, J. Phys. Condens. Matter 32 (2020) 135503, https://doi.org/10.1088/1361-648X/ab5f37.

[21] J. Li, H. Yin, N. Gao, M. Zhang, J. Mu, L. Gao, H. Li, First-principles calculations for Li, P dopants and vacancy defect in ultra-thin hydrogenated diamond nanofilms: structural, electronic and optical properties, Diamond Relat. Mater. 99 (2019) 107526, https://doi.org/10.1016/j.diamond.2019.107526.

[22] W. Li, X. Qian, J. Li, Phase transitions in 2D materials, Nat. Rev. Mater. (2021), https://doi.org/10.1038/s41578-021-00304-0.

[23] P.B. Sorokin, B.I. Yakobson, Two-dimensional diamond—diamane: current state and further prospects, Nano Lett. 21 (2021) 5475–5484, https://doi.org/10.1021/acs.nanolett.1c01557.

[24] K. Momeni, N. Sakib, D.E. Cintron Figueroa, S. Paul, C.Y. Chen, Y.-C. Lin, J. A. Robinson, Combined experimental and computational insight into the role of substrate in the synthesis of two-dimensional WSe2, ACS Appl. Mater. Interfaces 16 (2024) 6644–6652, https://doi.org/10.1021/acsami.3c16761.

[25] S. Paul, R. Torsi, J.A. Robinson, K. Momeni, Effect of the substrate on MoS_2 monolayer morphology: an integrated computational and experimental study, ACS Appl. Mater. Interfaces 14 (2022) 18835–18844, https://doi.org/10.1021/acsami.2c03471.

[26] P.V. Bakharev, M. Huang, M. Saxena, S.W. Lee, S.H. Joo, S.O. Park, J. Dong, D. C. Camacho-Mojica, S. Jin, Y. Kwon, M. Biswal, F. Ding, S.K. Kwak, Z. Lee, R. S. Ruoff, Chemically induced transformation of chemical vapour deposition grown bilayer graphene into fluorinated single-layer diamond, Nat. Nanotechnol. 15 (2020) 59–66, https://doi.org/10.1038/s41565-019-0582-z.

[27] S. Paul, K. Momeni, Mechanochemistry of stable diamane and atomically thin diamond films synthesis from bi- and multilayer graphene: a computational study, J. Phys. Chem. C 123 (2019) 15751–15760, https://doi.org/10.1021/acs.jpcc.9b02149.

[28] L.Y. Antipina, P.B. Sorokin, Converting chemically functionalized few-layer graphene to diamond films: a computational study, J. Phys. Chem. C 119 (2015) 2828–2836, https://doi.org/10.1021/jp510390b.

[29] Y. Gao, T. Cao, F. Cellini, C. Berger, W.A.D. Heer, E. Tosatti, E. Riedo, A. Bongiorno, Ultrahard carbon film from epitaxial two-layer graphene, Nat. Nanotechnol. 13 (2018).

[30] D. Odkhuu, D. Shin, R.S. Ruoff, N. Park, Conversion of multilayer graphene into continuous ultrathin sp^3-bonded carbon films on metal surfaces, Sci. Rep. 3 (2013) 51, https://doi.org/10.1038/srep03276.

[31] A.G. Kvashnin, P.B. Sorokin, Lonsdaleite films with nanometer thickness, J. Phys. Chem. Lett. 5 (2014) 541–548, https://doi.org/10.1021/jz402528q.

[32] L.A. Chernozatonskii, P.B. Sorokin, A.A. Kuzubov, B.P. Sorokin, A.G. Kvashnin, D. G. Kvashnin, P.V. Avramov, B.I. Yakobson, Influence of size effect on the electronic and elastic properties of diamond films with nanometer thickness, J. Phys. Chem. C 115 (2010) 132–136, https://doi.org/10.1021/jp1080687.

[33] H. Xie, F. Yin, T. Yu, J.-T. Wang, C. Liang, Mechanism for direct graphite-to-diamond phase transition, Sci. Rep. 4 (2014) 5930.

[34] S. Cai Zhu, X. Zhi Yan, J. Liu, A.R. Oganov, Q. Zhu, A revisited mechanism of the graphite-to-diamond transition at high temperature, Matter 3 (2020) 864–878, https://doi.org/10.1016/J.MATT.2020.05.013.

[35] R.Z. Khaliullin, H. Eshet, T.D. Kühne, J. Behler, M. Parrinello, Nucleation mechanism for the direct graphite-to-diamond phase transition, Nat. Mater. 10 (2011) 693–697, https://doi.org/10.1038/nmat3078.

[36] P. Xiao, G. Henkelman, Communication: from graphite to diamond: reaction pathways of the phase transition, J. Chem. Phys. 137 (2012), https://doi.org/10.1063/1.4752249.

[37] S. Scandolo, M. Bernasconi, G.L. Chiarotti, P. Focher, E. Tosatti, Pressure-induced transformation path of graphite to diamond, Phys. Rev. Lett. 74 (1995) 4015–4018, https://doi.org/10.1103/PhysRevLett.74.4015.

[38] K. Luo, B. Liu, W. Hu, X. Dong, Y. Wang, Q. Huang, Y. Gao, L. Sun, Z. Zhao, Y. Wu, Y. Zhang, M. Ma, X.-F. Zhou, J. He, D. Yu, Z. Liu, B. Xu, Y. Tian, Coherent interfaces govern direct transformation from graphite to diamond, Nature 607 (2022) 486–491, https://doi.org/10.1038/s41586-022-04863-2.

[39] S. Paul, K. Momeni, V.I. Levitas, Shear-induced diamondization of multilayer graphene structures: a computational study, Carbon N. Y. 167 (2020) 140–147, https://doi.org/10.1016/j.carbon.2020.05.038.

[40] K. Tong, X. Zhang, Z. Li, Y. Wang, K. Luo, C. Li, T. Jin, Y. Chang, S. Zhao, Y. Wu, Y. Gao, B. Li, G. Gao, Z. Zhao, L. Wang, A. Nie, D. Yu, Z. Liu, A.V. Soldatov, W. Hu, B. Xu, Y. Tian, Structural transition and migration of incoherent twin boundary in diamond, Nature 626 (2024) 79–85, https://doi.org/10.1038/s41586-023-06908-6.

[41] S.V. Erohin, Q. Ruan, P.B. Sorokin, B.I. Yakobson, S.V. Erohin, Q. Ruan, B. I. Yakobson, P.B. Sorokin, Nano-thermodynamics of chemically induced graphene–diamond transformation, Small 16 (2020) 2004782, https://doi.org/10.1002/SMLL.202004782.

[42] H. Sumiya, H. Yusa, T. Inoue, H. Ofuji, T. Irifune, Conditions and mechanism of formation of nano-polycrystalline diamonds on direct transformation from graphite and non-graphitic carbon at high pressure and temperature, High Press. Res. 26 (2006) 63–69, https://doi.org/10.1080/08957950600765863.

[43] K. Momeni, V.I. Levitas, A phase-field approach to nonequilibrium phase transformations in elastic solids: via an intermediate phase (melt) allowing for interface stresses, Phys. Chem. Chem. Phys. 18 (2016) 12183–12203, https://doi.org/10.1039/c6cp00943c.

[44] K. Momeni, V.I. Levitas, Propagating phase interface with intermediate interfacial phase: phase field approach, Phys. Rev. B. 89 (2014) 184102, https://doi.org/10.1103/PhysRevB.89.184102.

[45] K. Momeni, V.I. Levitas, J.A. Warren, The strong influence of internal stresses on the nucleation of a nanosized, deeply undercooled melt at a solid–solid phase interface, Nano Lett. 15 (2015) 2298–2303, https://doi.org/10.1021/nl504380c.

[46] Y. Peng, F. Wang, Z. Wang, A.M. Alsayed, Z. Zhang, A.G. Yodh, Y. Han, Two-step nucleation mechanism in solid–solid phase transitions, Nat. Mater. 14 (2014) 101–108, https://doi.org/10.1038/nmat4083.

[47] V.I. Levitas, K. Momeni, Solid–solid transformations via nanoscale intermediate interfacial phase: multiple structures, scale and mechanics effects, Acta Mater. 65 (2014) 125–132, https://doi.org/10.1016/j.actamat.2013.11.051.

[48] K. Momeni, V.I. Levitas, A phase-field approach to solid–solid phase transformations via intermediate interfacial phases under stress tensor, Int. J. Solids Struct. 71 (2015) 39–56, https://doi.org/10.1016/j.ijsolstr.2015.05.027.

[49] N. Sakib, S. Paul, N. Nayir, A.C.T. van Duin, S. Neshani, K. Momeni, Role of tilt grain boundaries on the structural integrity of WSe_2 monolayers, Phys. Chem. Chem. Phys. 24 (2022) 27241–27249, https://doi.org/10.1039/D2CP03492A.

[50] H. Attariani, S.E.E. Rezaei, K. Momeni, Mechanical property enhancement of one-dimensional nanostructures through defect-mediated strain engineering, Extrem. Mech. Lett. 27 (2019) 66–75, https://doi.org/10.1016/j.eml.2019.01.004.

[51] H. Attariani, S. Emad Rezaei, K. Momeni, Defect engineering, a path to make ultra-high strength low-dimensional nanostructures, Comput. Mater. Sci. 151 (2018), https://doi.org/10.1016/j.commatsci.2018.05.005.

[52] H. Attariani, K. Momeni, K. Adkins, Defect engineering: a path toward exceeding perfection, ACS Omega 2 (2017), https://doi.org/10.1021/acsomega.6b00500.

[53] M. Ghosh, S. Ghosh, H. Attariani, K. Momeni, M. Seibt, G. Mohan Rao, Atomic defects influenced mechanics of II-VI nanocrystals, Nano Lett. 16 (2016), https://doi.org/10.1021/acs.nanolett.6b00571.

[54] L.A. Varlamova, S.V. Erohin, P.B. Sorokin, The role of structural defects in the growth of two-dimensional diamond from graphene, Nanomaterials 12 (2022) 3983, https://doi.org/10.3390/nano12223983.

[55] K. Momeni, Y. Ji, N. Nayir, N.N. Sakib, H. Zhu, S. Paul, T.H. Choudhury, S. Neshani, A.C.T.T. Van Duin, J.M. Redwing, L.-Q.Q. Chen, A computational framework for guiding the MOCVD-growth of wafer-scale 2D materials, npj Comput. Mater. 8 (2022) 249, https://doi.org/10.1038/s41524-022-00936-y.

[56] K. Momeni, Y. Ji, Y. Wang, S. Paul, S. Neshani, D.E. Yilmaz, Y.K. Shin, D. Zhang, J.-W. Jiang, H.S. Park, S. Sinnott, A. van Duin, V. Crespi, L.-Q. Chen, Multiscale computational understanding and growth of 2D materials: a review, Npj Comput. Mater. 6 (2020) 22, https://doi.org/10.1038/s41524-020-0280-2.

[57] K. Momeni, Y. Ji, K. Zhang, J.A. Robinson, L.-Q. Chen, Multiscale framework for simulation-guided growth of 2D materials, Npj 2D Mater. Appl. 2 (2018) 27, https://doi.org/10.1038/s41699-018-0072-4.

[58] A. Shekhawat, R.O. Ritchie, Toughness and strength of nanocrystalline graphene, Nat. Commun. 7 (2016) 1–8, https://doi.org/10.1038/ncomms10546, 2015 71.

[59] A. Shekhawat, C. Ophus, R.O. Ritchie, A generalized Read–Shockley model and large scale simulations for the energy and structure of graphene grain boundaries, RSC Adv. 6 (2016) 44489–44497, https://doi.org/10.1039/C6RA07584C.

[60] C. Ophus, A. Shekhawat, H. Rasool, A. Zettl, Large-scale experimental and theoretical study of graphene grain boundary structures, Phys. Rev. B-Condens. Matter Mater. Phys. 92 (2015), https://doi.org/10.1103/PhysRevB.92.205402.

[61] Y. Liu, E. Project ALICE, I. Feng Sun, D. Yan, On centroidal Voronoi tessellation-energy smoothness and fast computation, ACM Ref. Format. 28 (2009), https://doi.org/10.1145/1559755.1559758.

[62] J. Zhang, J. Zhao, J. Lu, Intrinsic strength and failure behaviors of graphene grain boundaries, ACS Nano 6 (2012) 2704–2711, https://doi.org/10.1021/nn3001356.

[63] H. Los, A. Fasolino, Intrinsic long-range bond-order potential for carbon: performance in Monte Carlo simulations of graphitization, Phys. Rev. B-Condens. Matter Mater. Phys. 68 (2003) 1–14, https://doi.org/10.1103/PhysRevB.68.024107.

[64] S. Nosé, M.L. Klein, Constant pressure molecular dynamics for molecular systems 50, 2006, pp. 1055–1076, https://doi.org/10.1080/00268978300102851.

[65] S. Nosé, A unified formulation of the constant temperature molecular dynamics methods, J. Chem. Phys. 81 (1998) 511, https://doi.org/10.1063/1.447334.

[66] K. Momeni, H. Attariani, R.A.R.A. Lesar, Structural transformation in monolayer materials: a 2D to 1D transformation, Phys. Chem. Chem. Phys. 18 (2016) 19873–19879, https://doi.org/10.1039/c6cp04007a.

[67] K. Momeni, H. Attariani, Electromechanical properties of 1D ZnO nanostructures: Nanopiezotronics building blocks, surface and size-scale effects, Phys. Chem. Chem. Phys. 16 (2014), https://doi.org/10.1039/c3cp54456g.

[68] E.A. Belenkov, V.A. Greshnyakov, Modeling of phase transitions of graphites to diamond-like phases, Phys. Solid State 60 (2018) 1294–1302, https://doi.org/10.1134/S1063783418070065.

[69] V.A. Greshnyakov, E.A. Belenkov, Formation of diamond-like phases from hexagonal and tetragonal graphene layers, Bull. Russ. Acad. Sci. Phys. 82 (2018) 1209–1213, https://doi.org/10.3103/S1062873818090137.

[70] V.A. Greshnyakov, E.A. Belenkov, Simulation of the phase transition of graphite to the diamond-like LA3 phase, Tech. Phys. 61 (2016) 1462–1466, https://doi.org/10.1134/S1063784216100133.

[71] A.A. Shul'zhenko, L. Jaworska, A.N. Sokolov, V.G. Gargin, N.N. Belyavina, Phase transformations of n-layer graphenes into diamond at high pressures and temperatures, J. Superhard Mater. 39 (2017) 75–82, https://doi.org/10.3103/S1063457617020010.

[72] V.I. Levitas, D.L. Preston, Three-dimensional Landau theory for multivariant stress-induced martensitic phase transformations.I.Austenite(formula presented) martensite, Phys. Rev. B. 66 (2002) 134206, https://doi.org/10.1103/PhysRevB.66.134206.